This article has been accepted for inclusion in a future issue of this journal. Content is final as presented, with the exception of pagination.

Improved Biomass Calibration and Validation With Terrestrial LiDAR: Implications for Future LiDAR and SAR Missions

Atticus E. L. Stovall and Herman H. Shugart

***Abstract*—Future NASA and ESA satellite missions plan to better quantify global carbon stocks through detailed observations of forest structure, but ultimately rely on uncertain ground measurement approaches for calibration and validation. A substantial amount of uncertainty in estimating plot-level biomass can be attributed to inadequate and unrepresentative allometric relationships used to convert plot-level tree measurements to estimates of aboveground biomass. These allometric equations are known to have high errors and biases, particularly in carbon-rich forests, because they were calibrated with small and often biased samples of destructively harvested trees. To overcome this issue, we present and test a framework for nondestructively estimating tree and plot-level biomass with terrestrial laser scanning (TLS). We modeled 243 trees from 12 species with TLS and created ten low-RMSE allometric equations. The full 3-D reconstructions, TLS allometry, and Jenkins *et al.* (2003) allometry were used to calibrate SAR- and LiDAR-based empirical biomass models to investigate the potential for improved accuracy and reduced uncertainty. TLS reduced plot-level RMSE from 18.5% to 9.8% and revealed a systematic negative bias in the national equations. At the calibration stage, allometric uncertainty accounted for 2.8–28.4% of the total RMSE, increasing in relative contribution as calibration improved with sensor fusion. Our findings suggest that TLS plot acquisitions and nondestructive allometry can play a vital role for reducing uncertainty in calibration and validation data for biomass mapping in the upcoming NASA and ESA missions.**

***Index Terms*—Carbon, forestry, laser applications, uncertainty.**

I. Introduction

FORESTS provide essential ecosystem services and hold the vast majority of terrestrial carbon, but remain the most uncertain components of the carbon cycle [1]. Efforts to quantify the massive and dynamic storage of global carbon with a higher degree of certainty have revealed discrepancies arising from differing approaches [2], [3]. Disagreement in the magnitude of these distributions emphasizes the weak link in carbon mapping stems from individual tree and aggregated plot-level biomass estimates that are not representative [4]. Biomass estimates are derived from equations built from laborious destructive sampling of individual trees [5]. The inherent difficulty surrounding destructive harvesting of trees leads to insufficient sample sizes that produce unrepresentative spatially biased equations, rarely including large trees [6]. Before global carbon mapping can be improved, a substantial progress must be made in creating more representative allometry that will improve the accuracy of plot-level estimates of biomass.

Three-dimensional forest structure quantification is required for effective ecosystem service management and understanding current and future global carbon dynamics [1]. Global datasets capturing cover at coarse (MODIS) and fine (Landsat) spatial scales have allowed us to monitor forest status, but global information on the 3-D structure is insufficient for fine-scale management of essential ecosystem services [7]. Accurate mapping of more complex ecosystem characteristics such as biomass requires higher spatial resolution and information on the forest structure [8]. Globally distributed high-resolution 3-D data will provide the necessary information for managing ecosystems and constraining future climate projections [9].

Airborne sensors are often used to calibrate spaceborne sensors, but accuracy is dependent on quality plot-level biomass estimates. NASA's Land, Vegetation, and Ice Sensor is capable of capturing fine-scale 3-D vegetation structure that can simulate Global Ecosystem Dynamics Investigation (GEDI) and ICESAT-2 (Ice, Cloud, and land Elevation Satellite) data, allowing investigation of the instrument-specific response in a range of forest ecosystems prior to mission launch. Similarly, the synthetic aperture radar (SAR) used on UAVSAR can inform calibration of spaceborne pol-InSAR, such as NASA–ISRO SAR or the European Space Agency's BIOMASS mission. The success of these missions is directly dependent on accurate plot-level estimates of biomass that will ultimately improve confidence in landscape-scale mapping. Precise and unbiased estimates of biomass at the plot level are an essential component to improving carbon estimation with all future missions estimating global carbon. However, errors in plot-level biomass from unrepresentative allometry are unavoidable when relying on traditional field measurements for calibration and validation.

The empirical relationships used to relate tree diameter and height to biomass, or allometry, are known to be spatially variable [10] and not representative at low sample sizes [6], [11]. The solution to high variability in allometry has been the

Manuscript received September 26, 2017; revised January 5, 2018; accepted February 3, 2018. This work was supported by the NASA Virginia Space Grant Consortium (VSGC FY14-16, A. E. L. Stovall) and by the National Fish and Wildlife Foundation (0106.14.045246). *(Corresponding author: Atticus E. L. Stovall.)*

The authors are with the Department of Environmental Sciences, University of Virginia, Charlottesville, VA 22903 USA (e-mail: aes2aj@virginia.edu; hhs@virginia.edu).

Color versions of one or more of the figures in this paper are available online at http://ieeexplore.ieee.org.

Digital Object Identifier 10.1109/JSTARS.2018.2803110

1939-1404 © 2018 IEEE. Personal use is permitted, but republication/redistribution requires IEEE permission.
See http://www.ieee.org/publications_standards/publications/rights/index.html for more information.

This article has been accepted for inclusion in a future issue of this journal. Content is final as presented, with the exception of pagination.

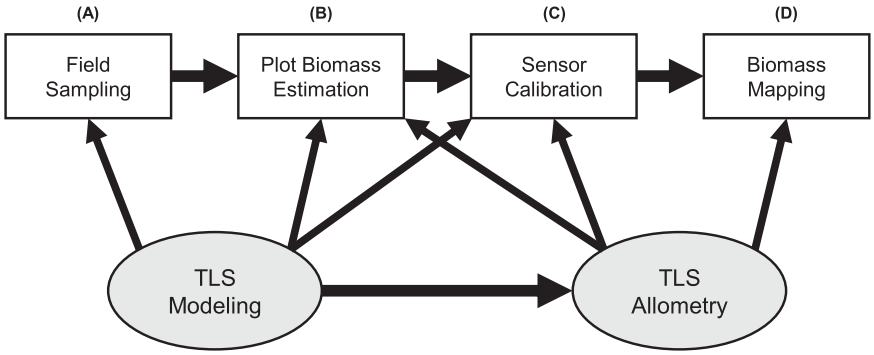

Fig. 1. Framework for reducing uncertainty with targeted TLS acquisition through modeling and improved allometry. At each step of biomass mapping, TLS can potentially improve the current methodology. (a) At the stage of field sampling, TLS is an efficient and relatively unbiased method of collecting standard forest structure information (e.g., DBH, height, basal area, and vegetation area index). (b) Plot-level biomass estimation can be improved through direct stem modeling with TLS or nondestructive local allometry with TLS. (c) TLS can potentially improve sensor calibration and validation through full plot-level 3-D reconstruction. Reduced uncertainty biomass allometry can be applied regionally, further improving sensor calibration. (d) Low-uncertainty sensor calibration will provide the greatest potential for reducing uncertainty in biomass mapping.

pooling of massive datasets globally to create stable equations that are not species specific [12]. While this approach is acceptable for coarse estimates of forest biomass, it is insufficient for calibration and validation plot-level data for GEDI and other missions as they must have high accuracy and precision because nonspecies-specific equations can have greater than 350% error [13], emphasizing the importance of equation selection [14]. Improvement in allometric equations is one way to substantially improve calibration and validation plot data, since it does not require resampling and can be applied across large areas, but the inherent difficulties surrounding destructive sampling limit the feasibility of this approach. Efficient, automated, and nondestructive methods of estimating aboveground biomass of single trees, such as terrestrial LiDAR, offer a solution to the problems of unrepresentative allometry.

Terrestrial laser scanning (TLS) or terrestrial LiDAR is the best current method of nondestructively estimating single-tree and plot-level biomass in a range of ecosystems [15], [16]. TLS recreates a plot-level structure with millimeter detail, allowing for 3-D reconstruction of tree stems with geometric modeling [17]. TLS has been deployed in most of the forest ecosystem types, successfully estimating tree volume and biomass with lower error than allometric equations [15], [18]. Calibration and validation plot data can be improved by applying TLS as a tool for estimating plot-level biomass with higher accuracy than allometric equations. Moreover, nondestructive tree modeling with TLS offers the potential for unbiased and high-sample-size allometry that can include trees of any size with minimal effort. The greatest improvements to calibration and validation data are surely to come in tropical forests where region-specific and species-specific allometries are extremely rare. While deploying TLS for direct plot-level biomass estimation and the creation of area-specific allometry will likely reduce uncertainty in plot-level biomass estimates used for calibration and validation, it is still unclear whether or not this will result in major differences at the level of sensor calibration.

This study presents TLS as a potential approach to improving airborne and satellite-based biomass calibration and validation through direct structural measurements and improved allometric equation development (see Fig. 1). We investigate TLS in this context by:

1) directly modeling plot-level tree biomass and developing high-sample-size nondestructive local biomass allometry for the dominant species groupings in a broadleaf deciduous hardwood forest;
2) using both direct and allometrically derived TLS biomass estimates for calibrating an empirical plot biomass model with SAR and LiDAR;
3) comparing the uncertainty of the biomass models to an equivalent approach relying on the national-scale Jenkins *et al.* [19] biomass allometry.

II. Methods

A. Study Area and Species Selection

The study site is the 25.6 ha (400 m $\times$ 600 m) Smithsonian Institute Global Earth Observatory (SIGEO) temperate Large Forest Dynamics Plot in the Smithsonian Conservation Biology Institute near Front Royal, VA (38°53'36.6" N, 78°8'43.4" W; Fig. 2). This mixed deciduous hardwood forest is nearly 100 years old and representative of many on the east coast of the U.S. experiencing postagricultural regrowth. Elevation ranges from 273–338 m and mean annual temperature and precipitation for the area are 12.7 °C and 970 mm, respectively. This SIGEO site was intensively sampled in 2010 for species, diameter, and stem location from a dataset of over 56 000 individuals greater than 1-cm diameter at breast height (DBH) [20]. We used the *a priori* forest structure information to determine the most important species for biomass analysis based on available allometry. The dominant species contributing biomass to the forest with average wood density values ($g{\cdot}cm^{-3}$) were: *Liriodendron tulipifera* (0.40), *Carya cordiformis* (0.62), *Carya glabra* (0.62), *Carya ovalis* (0.62), *Carya tomentosa* (0.62), *Fagus grandifolia* (0.56), *Fraxinus americana* (0.55), *Nyssa sylvatica* (0.46), *Quercus alba* (0.60), *Quercus prinus* (0.57), *Quercus rubra* (0.56), and *Quercus velutina* (0.56) [21]. These species

This article has been accepted for inclusion in a future issue of this journal. Content is final as presented, with the exception of pagination.

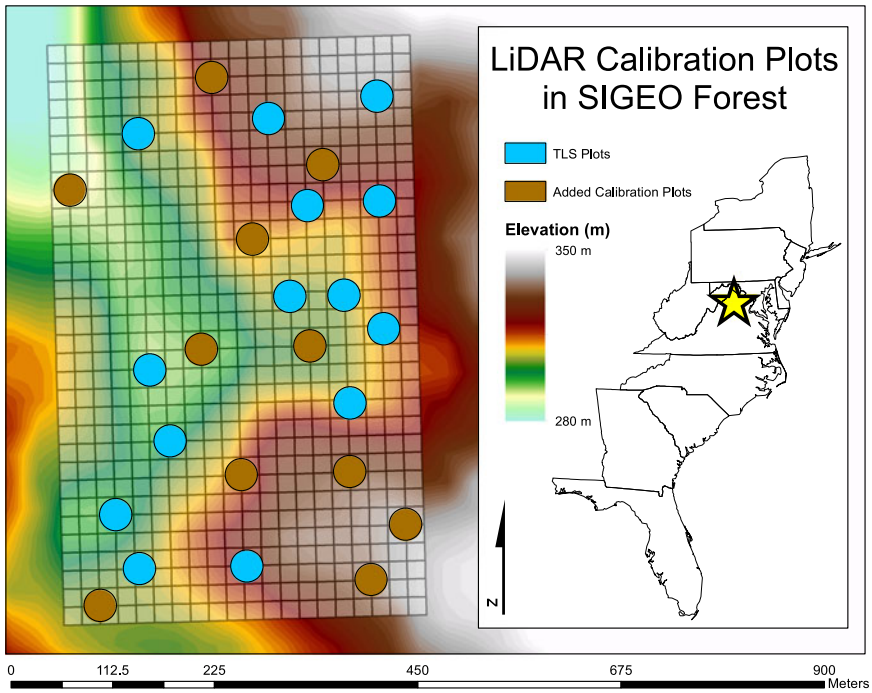

Fig. 2. Overview map of SIGEO forest at the Smithsonian Conservation Biology Institute in Front Royal, VA ($\star$). Fourteen randomly distributed 1/10th ha circular plots (shown to scale) were located on the 20-m grid intersections and scanned with TLS (blue). Eleven additional plots were included for SAR and LiDAR calibration (brown). An elevation model derived from the 2011 LiDAR acquisition shows the topography across the site. Note: TLS plots are positioned off center from the shown grid intersections, as these locations were georeferenced to the LiDAR canopy height model.

were used for nondestructive TLS-based local allometric equation development described in the subsequent sections, as they were estimated to contribute over 80% of aboveground forest biomass.

B. TLS Allometry

1) TLS Sampling and Postprocessing: Within the SIGEO forest, we chose 14 1/10th ha circular (radius $\approx$ 17.8 m) plot sampling locations at random using ArcGIS mapping software. TLS sampling took place over four days in April of 2015 during leaf-off conditions. Individual plots were located using a handheld Garmin eTrex GPS unit, and plot centers were found on the marked 20-m grid intersections of the SIGEO plot grid network. The Faro Focus 120 3-D phase-shift TLS was set to medium resolution and quality (1/5 resolution and 4$\times$ quality) for a total of 28.2 million pulses per scan. Time elapsed per scan was approximately 3 min. We reduced occlusion from the presence of high-density vegetation by scanning five times in a diamond pattern oriented at approximately each cardinal direction to provide sufficient coverage and a standardized sampling scheme. At times, an additional scan was required for full coverage. To aid in postprocessing scan registration, we placed 6-in-diameter polystyrene spheres atop fiberglass stakes throughout the plot. Multiple scans were digitally registered using the registration points, as described in the following section.

2) Postprocessing: Individual scans were registered using the automatic registration algorithms included in Faro SCENE [22], and overlapping redundant points were filtered to create a single 3-D point cloud used for modeling. The registration process relied on the spheres used on each field plot. Spheres were located in every scan and aligned with each corresponding sphere in other scans from the same plot. We evaluated plot-level registration error in SCENE to ensure precise scan placement (mean = 4.5 mm, sd = 4.8 mm, and max = 14 mm). While phase-shift TLS is less expensive and provides fast high-resolution scans, the technology is susceptible to noise on edges and close to the range limit. To improve the scan quality, we filtered scans by removing all returns below the intensity threshold of 400. A stray point filter included in the Faro software was then used to remove ambiguous points at the edges of vegetation. The registered point cloud data were then exported with column and row numbers, which correspond to scan azimuth and angle, as well as intensity values ranging from 0 to 2100. Registered plot-level point clouds typically had approximately 100 million returns in closed canopy forest. TLS can reduce the geolocation error when paired with airborne LiDAR, mitigating some of the uncertainty in the calibration stage [23]. We minimized errors in plot GPS locations by manually georeferencing TLS data to a 1-m LiDAR-derived canopy height model. To accomplish this, each registered TLS cloud was placed at the initial coordinates of the grid intersection and adjusted in the xyz space until the top-of-canopy returns in the TLS cloud aligned with the LiDAR model (Blue plots, Fig. 2).

3) Volume and Biomass Estimation: We separated and modeled individual trees on each plot using an automated workflow within the CompuTree software [24]. The processing took place in four steps: ground point classification and DTM creation,

This article has been accepted for inclusion in a future issue of this journal. Content is final as presented, with the exception of pagination.

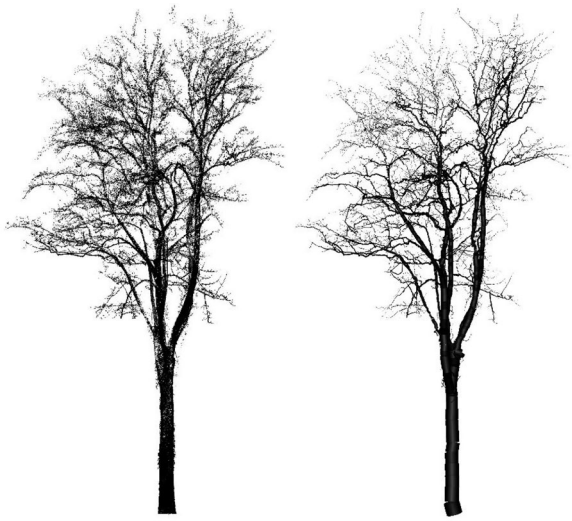

Fig. 3. Example (a) TLS point cloud from a 120-cm-diameter *Liriodendron tulipifera* and the resulting (b) 3-D TLS model.

stem identification, tree segmentation, and stem reconstruction with quantitative structure models (QSMs) (see Fig. 3). The ground points were classified with a local minima ground estimation algorithm, which reconstructs the DTM, while excluding aboveground points associated with vegetation. Stems were identified using a nearest neighbor and connected component approach on a small slice in the point cloud made parallel to the DTM. Stems spaced apart from one another were identified as a unique object, and this portion of the point serves as the initial seed point to initiate the cylinder modeling algorithm implemented in SimpleTree [18]. The tree was then automatically segmented from the point cloud using an iterative nearest neighbor approach, starting at the initial seed point on the stem and moving vertically while expanding in area with the expanding tree crown. The segmented tree was then reconstructed through cylinder fitting with the QSM algorithm. The best-fit cylinders were used as a guide for creating an allometric relationship between trunk size and branching order—an adaptation of the pipe model concept or scaling theory [25]. This single-tree relationship guided all low-certainty cylinder measurements, filling gaps in the tree model with likely cylinder sizes that correspond to the expected branching order. As a result, tree reconstructions have low variability between model runs because whole-tree estimates are primarily based on high-quality cylinder measurements. This approach as implemented in SimpleTree was validated with a number of destructive samples and accurately estimated biomass with approximately 10–15% RMSE [18]. Based on the previous success of these algorithms in similar forest systems in leaf-off conditions, we anticipated this application in our forest to be comparable in accuracy and precision.

The cylinder models (referred to as TLS models hereafter) provided an estimate of volume, which were converted to estimates of biomass using

$$\text{Biomass} = \rho_s \, V_{\text{TLS}} \tag{1}$$

where V_{TLS} is the modeled volume (cm^3) and ρ_s is the average species specific wood density ($\text{g}\cdot\text{cm}^{-3}$) reported in the literature [21]. Since we were unable to validate the TLS models with destructive samples at this study site, the uncertainty of the TLS-based volume estimates was assumed to be comparable to a previous study in similar leaf-off conditions (11.38%) [18]. Biomass estimates were converted to kilograms for direct comparison to other allometric equations.

While small-scale biomass mapping is unlikely to show wide variation in species-specific wood density, we attempted to capture potential species-specific variability in our TLS models. Legacy Tree Data is an in-progress compilation of thousands of tree-level measurements from across the United States [26]. We used Legacy Tree Data to collect whole-tree wood density measurements from 359 trees sampled in Virginia and surrounding states covering all of our study species except *Fagus grandifolia* (data unavailable) [27]–[29]. Measured species-specific wood density was within 5% of the average values reported in [21]. Measured values had an average standard deviation across all species of 0.027 (g/cm^3) or 5%. We incorporated this variability in species-specific wood density in the uncertainty of the TLS models to more accurately capture uncertainty using this method of biomass estimation. For a simple analysis of species and density effects on volume and biomass estimates, we stratified our allometric models by these two factors and quantified the improvements in RMSE in each case. This approach of disentangling density effects may be beneficial to future national-scale biomass estimation, allowing density-dependent allometry, along with uncertainty, to be captured and used across large areas.

4) Allometric Equation Development: Allometric relationships were developed from the TLS biomass estimates with a log-linear regression method taking the form

$$\hat{B}_{\text{tree}} = \exp\left(\beta_0 + \beta_1 * \ln\left(\text{DBH}\right)\right) + \epsilon_{\text{tree}} \tag{2}$$

where β_0 and β_1 are the model coefficients and ϵ_{tree} is the residual error from the allometric equation. We created diameter–height allometry from the same set of trees with the form

$$\hat{B}_{\text{tree}} = \exp\left(\beta_0 + \beta_1 * \ln\left(\text{DBH}^2 \; H\right)\right) + \epsilon_{\text{tree}} \tag{3}$$

Considering that the predictor, $\text{DBH}^2 \; H$, is proportional to columnar wood volume, the final equations were approximately linear, but log transformed in order to satisfy the assumption of homoscedasticity for least-squares regression. Height was not directly measured across all trees at the site, so an allometric model was built in the same form as (2), substituting tree height for biomass. Trees with direct TLS-based measurements of height were assumed to have a zero error, but for allometric height estimates, we included this uncertainty in the model.

Modeled trees were grouped into five different equations: *Liriodendron*, *Carya*, *Quercus*, Mixed Hardwood, and Maple/Oak/Hickory/Beech (see Table I). The groups were based on the dominant forest species (Poplar, Oak, and Hickory) and two general equations similar to groupings in [19] that could describe the remaining abundant species. TLS models of *Carya* species had a maximum diameter of 47 cm, so

This article has been accepted for inclusion in a future issue of this journal. Content is final as presented, with the exception of pagination.

TABLE I
GENERAL DIAMETER AND DIAMETER–HEIGHT ALLOMETRY INCLUDING THE TEN SPECIES MODELED WITH TLS

Form	Equation	Range (cm)	n	β_0	$\beta_0[se]$	β_1	$\beta_1[se]$	r^2	RMSE (CV)
DBH	**Lt**	13 – 120	47	−1.9136	0.17	2.3513	0.04	0.98	0.16
	Q	11 – 93	66	−1.5091	0.25	2.3237	0.07	0.95	0.24
	C	10 – 47	86	−2.2249	0.25	2.5765	0.08	0.92	0.31
	MH	11 – 120	77	−2.2647	0.16	2.4503	0.05	0.97	0.26
	MO	10 – 105	166	−1.6637	0.14	2.3787	0.04	0.95	0.29
DBH^{2}H	**Lt**	13 – 120	47	−3.1210	0.18	0.9263	0.02	0.99	0.15
	Q	11 – 93	66	−3.2444	0.25	0.9722	0.02	0.97	0.20
	C	10 – 47	86	−2.8364	0.23	0.9398	0.03	0.94	0.27
	MH	11 – 120	77	−2.9337	0.15	0.9135	0.01	0.98	0.22
	MO	10 – 105	166	−2.8783	0.13	0.9415	0.01	0.97	0.24

Equations were created for *Liriodendron tulipifera* (**Lt**), *Quercus* (**Q**), and *Carya* (**C**). The mixed hardwood equation (**MH**) includes *Fraxinus americana*, *Liriodendron tulipifera*, and *Nyssa sylvatica*. The Hard maple/Oak/Hickory/Beech equation (**MO**) includes *Quercus*, *Carya*, and *Fagus grandifolia*. RMSE is in log units and based on fivefold cross validation.

the Maple/Oak/Hickory/Beech equation was used for individuals that exceeded the Carya allometry diameter range. The high-biomass contribution of the ten species included in these allometric models increases the likelihood for changes to allometrically derived forest biomass under differing equations.

Several equation forms were evaluated in terms of coefficient of determination (R^2), Akakai information criterion (AIC) weights, and RMSE. While the diameter did not explain as much biomass variability as equations also including height, the diameter-only equation provided a clear comparison to the Jenkins *et al.* equations. Diameter–height equations were included to show the potential for reducing biomass uncertainty by including height in allometry. Model uncertainty of each allometric equation was reported in terms of RMSE in log units in order to reflect increasing uncertainty with increasing biomass and to directly compare to the Jenkins *et al.* equations' reported error. We performed a fivefold cross validation on each allometric equation to independently estimate uncertainty.

5) Biomass Estimation: We applied our nondestructive allometry and Jenkins *et al.* allometry to the diameter measurements of the trees located within each TLS plot. For those individuals that were not selected for updated allometry, the national equations were used in order to provide a biomass contribution in our assessment. We used biomass estimates from TLS models with TLS allometry, TLS diameter allometry, TLS diameter–height allometry, and Jenkins *et al.* allometry as our calibration datasets. The plot-level biomass estimates derived from the direct 3-D tree models were supplemented with TLS allometry or national-scale allometry if the individual was not successfully modeled, as was the case with many small trees in each plot. The national-scale equations were substituted if the species was not one of the 12 species included in the TLS allometry to ensure every individual contributed biomass regardless of the equation used. Aboveground biomass density (Mg·ha^{-1}) was estimated by aggregating tree estimates to the plot level using

$$\hat{B}_{\text{plot}} = \sum_{i=1}^{n_{\text{tree, plot}}} \hat{B}_{\text{tree},i}/s \tag{4}$$

where $n_{\text{tree,plot}}$ is the number of trees on a plot and s is the area of the plot in hectares. We propagate uncertainty due to allometry to the plot level with methods outlined in a previous study [30] using

$$\sigma_{\text{plot}} = \sqrt{\sum_{i=1}^{n_{\text{tree, plot}}} {\sigma_{\text{tree},i}}^2/s} \tag{5}$$

where $\sigma_{\text{tree},i}$ is the biomass error from allometric equation residuals.

C. SAR and LiDAR Biomass Calibration

1) SAR Data Source: Phased-Array-type L-band Synthetic Aperture Radar (PALSAR) data captured in the fine-beam dual-polarization mode with the Advanced Land Observing Satellite on January 5, 2011 was acquired for this study to investigate allometric uncertainty in calibration of SAR sensors for biomass estimation. The high-resolution radiometrically terrain-corrected PALSAR data product is radiometrically and geometrically corrected with the National Elevation Dataset to ensure that pixel values accurately represent backscatter from the reflecting surface and images are not distorted. Multilook processing degrades resolution by averaging over the slant range and/or azimuth while producing a 12.5-m-resolution square pixel raster. Coregistration was visually verified in the study area against high-resolution imagery by comparing isolated buildings in open areas and forest edges. Alignment was found to be accurately geolocated at the subpixel level. The horizontal send and vertical receive mode of the L-band SAR is strongly related to biomass up to approximately 150 Mg·ha^{-1} [31] and was used for biomass model calibration. All processing was completed by the Alaska Satellite Facility [32].

2) Airborne LiDAR Data Source: Airborne LiDAR data were acquired with the Optech 3100 instrument at approximately 1371 m above the ground level over an area overlapping the SIGEO forest from March 1–9, 2011 and extended nearly 2500 km^2 beyond our site. Nominal point spacing was 1 m, and up to four returns were recorded. The primary purpose of the LiDAR acquisition was high-resolution digital earth model (DEM) creation, so it was completed in leaf-off conditions at

This article has been accepted for inclusion in a future issue of this journal. Content is final as presented, with the exception of pagination.

this lower point spacing. Average horizontal and vertical errors were 37 and 6.6 cm, respectively.

3) SAR and LiDAR Metrics: Canopy height and SAR backscatter were used as two analogous variables to the upcoming satellite missions attempting to characterize global forest structure. The SAR backscatter (SAR_σ) can penetrate cloud cover and has a strong relationship with biomass in lower density environments. However, in high-biomass forests, the backscatter has a well-documented loss of sensitivity or "saturation." Considering the lack of low-biomass forest in our study area, we anticipated a high-uncertainty model with a limited predictive power. We attempted to improve the model by selecting eight open-field plots near the site with zero biomass to include in our calibration. The low-biomass plots were strictly used for calibration and were excluded in any evaluations of RMSE to avoid inflation of model statistics.

Canopy height will be captured with LiDAR (GEDI and ICESAT II) and PolInSAR or TomoSAR (BIOMASS and NISAR), thus making this structural variable essential for estimating biomass and quantifying the potential for uncertainty reduction with application of TLS. We used the Fusion LiDAR Data Toolkit to calculate canopy metrics. The processing was accomplished using the CloudMetrics algorithm. The mean canopy height (MCH) was calculated by first creating a 5-m-resolution DEM using all LiDAR ground returns. The LiDAR data were normalized to the DEM, subtracting the corresponding DEM elevation from the point cloud. Ground returns were removed with a simple 1-m height threshold above the DEM. The MCH was calculated as the mean height above the DEM of all returns above ground on each 1/10th ha circular plot. Additionally, the most frequent LiDAR return height (MODE), the number of fourth returns within a plot (4R), and the 99th percentile of return intensity (I) were calculated for a multiple regression model.

4) SAR and LiDAR Empirical Models: Two empirical model forms were used to estimate plot biomass relying on single linear regression for the individual LiDAR and SAR metrics—MCH and SAR_σ—and multiple linear regression for the combination of the two metrics. We included an additional model built from LiDAR-derived metrics using the MCH, as well as MODE, 4R, and intensity. The four models were created for each set of biomass estimation methods: TLS models, TLS diameter allometry, TLS diameter–height allometry, and Jenkins *et al.* allometry. The combination compared the four SAR- and LiDAR-based metrics and four methods of estimating biomass for a total of 16 empirical models. For each simple linear model, biomass ($\hat{B}_{\mathrm{plot}}$) was estimated using

$$\hat{B}_{\mathrm{plot}} = \beta_0 + \beta_1(\mathrm{MCH}, \mathrm{SAR}_\sigma) + \epsilon_{\mathrm{plot}} \tag{6}$$

where β_0 and β_1 are the model coefficients describing the relationship of LiDAR or SAR metrics (MCH or SAR_σ) to biomass. The error term ϵ_{plot} represents the residual error of the empirical biomass model. In the case of multiple regression, the model takes the form

$$\hat{B}_{\mathrm{plot}} = \beta_0 + \beta_1(\mathrm{MCH}) + \beta_2(\mathrm{SAR}_\sigma) + \epsilon_{\mathrm{plot}} \tag{7}$$

where β_1 and β_2 are coefficients for MCH and SAR_σ, respectively. The final four-variable model followed the form of (7), but used MCH, MODE, R4, and I, along with the corresponding coefficients (β_3 and β_4). Errors in estimating LiDAR metrics and model parameters contribute very little to the total uncertainty compared to the residual error in the calibration model [30] and were assumed to be negligible for this analysis. ϵ_{plot} is entirely derived from the residual error; however, given these formulations, plot biomass uncertainty is not accounted for. Any variation in ϵ_{plot} under differing allometric relationships will be due to changes in mean biomass density, rather than propagated allometric uncertainty. We quantify LiDAR model prediction uncertainty including the allometric error with

$$\sigma_{\mathrm{pred}}{}^2 = \sigma_{\epsilon,\mathrm{plot}}{}^2 + \sigma_{\epsilon,\hat{B}_{\mathrm{plot}}}{}^2 \tag{8}$$

where σ_{pred} is the total uncertainty from the empirical biomass model, $\sigma_{\epsilon,\mathrm{plot}}$ is the uncertainty due to LiDAR model residuals, and $\sigma_{\epsilon,\hat{B}_{\mathrm{plot}}}$ is the uncertainty propagated from allometric equations to the plot level. The sources described were the major contributors to biomass prediction uncertainty in a similar analysis quantifying most sources of uncertainty in biomass mapping [30].

III. Results

A. TLS Allometry

TLS successfully created ten different allometric equations using 243 3-D tree models. Small stems below 10 cm in diameter were difficult to accurately model so most were excluded in this study, but considering our interest in estimating biomass, we measured TLS modeling success by the total basal area captured per plot. On average, TLS modeled 70.6% of the plot basal area. A single plot was a strong outlier with extremely dense understory vegetation and only three trees successfully modeled with TLS. Removing this outlier increased the total plot basal area modeled with TLS to 92.9%. From the TLS models, three equations were created according to the dominant species across the site: *Liriodendron tulipifera*, *Quercus*, and *Carya*. Two additional equations encompassed the species included in the Jenkins *et al.* 2003 mixed hardwood (MH) and Hard maple/Oak/Hickory/Beech (MO) equations using a high number of TLS models. The additional equations were used for any individuals that were beyond the more specific equations diameter range in order to reduce bias in larger trees.

The grouping used in this study was based on the evaluation of multiple equation forms (data not shown). The diameter-based equation selected had the lowest AIC and highest AIC weight of all model forms tested. The inclusion of height reduced the RMSE across all equations. However, since height was not measured across the site, we estimated the height across the site with allometry derived from the TLS models (RMSE = 3.95 m, 17.3%). Initially, individual species equations were evaluated, but no significant differences in slopes were found across multiple species. All *Carya* species were statistically similar. Only *Quercus velutina* was significantly different in the *Quercus* equation grouping. The *Liriodendron tulipifera* equation was prioritized because of the presence of this species across

This article has been accepted for inclusion in a future issue of this journal. Content is final as presented, with the exception of pagination.

TABLE II
UNCERTAINTY OF 16 EMPIRICAL BIOMASS MODELS BASED ON CALIBRATION DATA FROM TLS MODELS (M), TLS DIAMETER–HEIGHT ALLOMETRY (DH), TLS DIAMETER ALLOMETRY (D), AND JENKINS *et al.* 2003 EQUATIONS

Model	Method	$\sigma_{\epsilon,\text{plot}}$	$\sigma_{\epsilon,\text{plot}}$ (%)	σ_{pred}	σ_{pred} (%)
$\beta_0 + \beta_1(\text{SAR}_\sigma)$	TLS (M)	119.0	38.9	123.0	40.2
	TLS (DH)	119.0	38.2	123.0	39.5
	TLS (D)	119.0	38.1	123.0	39.3
	Jenkins	125.0	45.3	128.0	46.6
$\beta_0 + \beta_1(\text{MCH})$	TLS (M)	54.7	17.9	62.4	20.4
	TLS (DH)	55.0	17.7	66.1	21.2
	TLS (D)	55.0	17.6	68.5	22.0
	Jenkins	63.2	23.0	81.1	29.5
$\beta_0 + \beta_1(\text{MCH}) + \beta_2(\text{SAR}_\sigma)$	TLS (M)	54.6	17.8	62.4	20.4
	TLS (DH)	55.2	17.7	66.3	21.2
	TLS (D)	55.2	17.7	68.6	22.0
	Jenkins	63.5	23.1	81.3	29.6
$\beta_0 + \beta_1(\text{MCH}) + \beta_2(\text{I}) +$ $\beta_3(\text{MODE}) + \beta_4(\text{4R})$	TLS (M)	40.8	13.3	50.7	16.6
	TLS (DH)	41.5	17.5	55.3	21.8
	TLS (D)	41.5	13.3	58.1	18.6
	Jenkins	52.1	19.0	72.8	26.5

Four models are compared using SAR backscatter (SAR_σ) and MCH, as well as two multiple regression models using both metrics and a suit of airborne LiDAR metrics—LiDAR intensity (I), most common return height (MODE), and number of fourth returns (4R). Model residual uncertainty ($\sigma_{\epsilon,\text{plot}}$) and propagated uncertainty ($\sigma_{\epsilon,\text{pred}}$) are reported in $\text{Mg}\cdot\text{ha}^{-1}$ and as a percentage of the mean (equivalent to the relative RMSE).

the site. To evaluate effects of species and density on biomass and volume estimates, we stratified our equations by these factors and tested for significant model improvement. Volume allocation differed across species, resulting in increased explanatory power in the diameter-based allometric model ($p < 0.001$), but when height was included species did not offer additional explanatory power ($p = 0.44$). Wood density has a strong effect on model precision, improving RMSE substantially for the diameter (0.33 versus 0.28, $p < 0.001$) and diameter–height (0.28 versus 0.22, $p < 0.001$) models.

The *Liriodendron tulipifera* equation had the lowest uncertainty (RMSE = 0.16) of all TLS allometry and the lowest equation sample size ($n = 47$; Table I). The *Carya* equation had the highest uncertainty (RMSE = 0.31) but the highest sample size for a single-species equation ($n = 86$). The MO equation had a high diameter range (10–105 cm) and the highest sample size ($n = 166$). The MH equation had the highest diameter range (11–120 cm) of all equations, and the slope coefficient (β_1) was similar to the Jenkins *et al.* MH equation (2.4503 versus 2.4835, respectively), but RMSE was lower (0.26 versus 0.36, respectively). Including height improved model fit and reduced uncertainty in all equations (see Table I).

B. Biomass Estimation and Uncertainty Analysis

Tree biomass estimations from TLS models with TLS allometry, TLS allometry, and Jenkins *et al.* allometry were aggregated to the plot level to be used for LiDAR and SAR empirical models. A total of 1818 trees were included on the TLS plots (blue, Fig. 2), but including the additional 11 plots for calibration increased the sample to 3947 trees. TLS-based biomass density was similar across all TLS-based methods with 306 ± 117 $\text{Mg}\cdot\text{ha}^{-1}$ for TLS models, 312 ± 120 $\text{Mg}\cdot\text{ha}^{-1}$ for TLS diameter allometry, and 311 ± 121 $\text{Mg}\cdot\text{ha}^{-1}$ for TLS diameter–height allometry, but Jenkins *et al.* estimates were lower (275 ± 126 $\text{Mg}\cdot\text{ha}^{-1}$). Relative plot uncertainty was lowest with TLS models (9.8%), followed by TLS diameter–height allometry (12.2%), TLS diameter allometry (13.1%), and Jenkins *et al.* allometry (18.5%). Uncertainty of the TLS diameter–height allometry reduced to 11.8% if height was assumed to be measured error-free, rather than estimated from diameter measurements.

For the empirically derived calibration models, the MCH outperformed the SAR backscatter as a predictor variable, but the combination had both lower uncertainty and bias (see Table II). Propagating allometric uncertainty to the LiDAR models increased model uncertainty in all cases. Use of TLS models over the Jenkins equations for calibration reduced model uncertainty through reduced plot-level uncertainty and lower residual error. For example, TLS models reduced the residual error by 5.4% and the propagated error by 9.7% in the MCH LiDAR model. TLS reduced uncertainty in all calibration models with the greatest reduction in the multiple regression model (9.9%). The relative contribution of error from allometry increased with improved LiDAR models (see Fig. 4). The most uncertain set of models (SAR_σ) had the lowest relative contribution of uncertainty from allometry (2.8–3.1%), while the least uncertain set (four-variable LiDAR model) had the highest relative contribution to uncertainty from allometry (19.6–28.4%).

IV. DISCUSSION

The framework presented in this study uses TLS to reduce uncertainty at multiple levels of biomass estimation. We compared uncertainty from plot-level 3-D stem reconstruction, TLS diameter allometry, TLS diameter–height allometry, and the Jenkins *et al.* 2003 equations. The five TLS-derived allometric equations created using 3-D stem models had low uncertainty and high sample size, making them suitable for application across other plots within the site. Plot uncertainty was estimated from the RMSE in the allometric equations and propagated to the empirical plot biomass relationship from LiDAR metrics. The source of the majority of biomass estimation

This article has been accepted for inclusion in a future issue of this journal. Content is final as presented, with the exception of pagination.

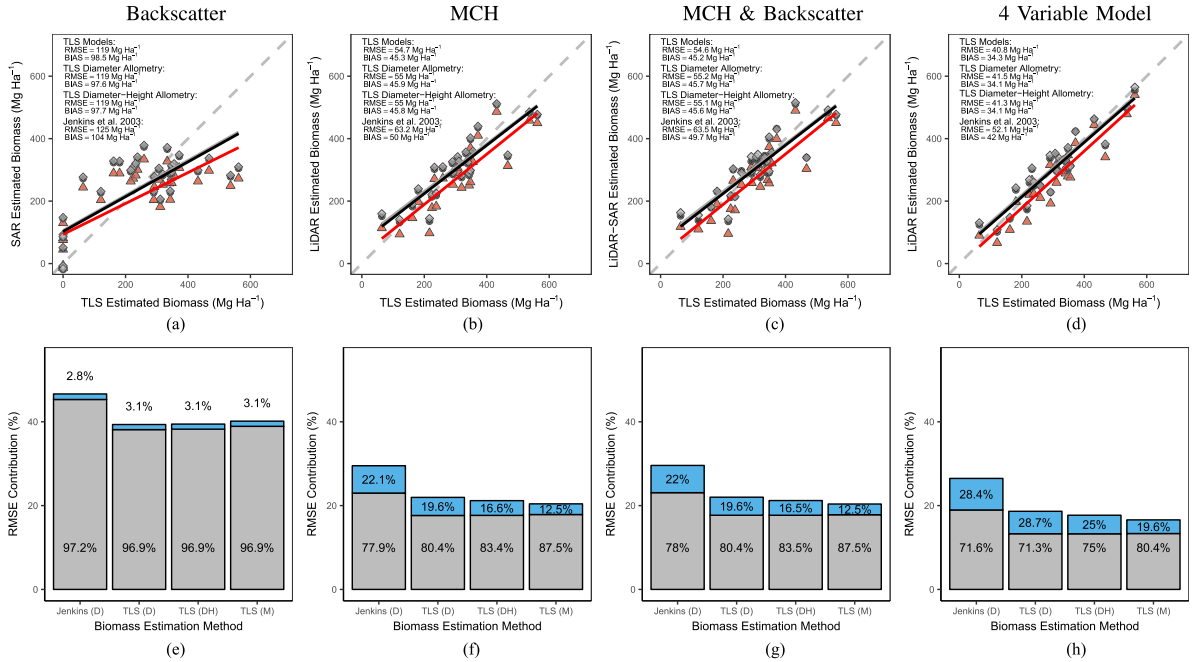

Fig. 4. Comparison of SAR and LiDAR biomass calibration models (top row) and propagated uncertainty of biomass estimates (bottom row). PALSAR backscatter was used as a representative metric captured with PolSAR missions [(b) and (f)]. MCH was used as a comparable canopy height metric collected using spaceborne LiDAR (GEDI or ICE-Sat II) [(b) and (f)]. MCH and backscatter were combined to emulate PolInSAR or TomoSAR (BIOMASS or NISAR) and potential cross-sensor fusion [(c) and (g)]. The final row [(d) and (h)] uses a calibration approach more common to airborne LiDAR, combining multiple height metrics (MCH, intensity, most frequent return height, and the number of fourth returns). The TLS models (black) provided the lowest uncertainty estimates, followed by TLS diameter–height allometry, TLS diameter allometry (gray), and Jenkins *et al.* 2003 allometry (red). TLS diameter–height allometry is not shown, as the trend and data points were indistinguishable from the TLS diameter allometry (gray). TLS reduced the total propagated uncertainty of LiDAR calibration by 10% (over 30% relative), with improvements in both plot-level and LiDAR calibration RMSE. Percentages within stacked bars indicate the relative contribution of uncertainty from allometry (blue) versus the LiDAR-derived empirical model (gray).

uncertainty was the residual error in the SAR and LiDAR calibration models, but allometry contributed 2.8–28.4% of the total uncertainty. A combined set of LiDAR metrics produced the best model with low uncertainty. In all cases, TLS reduced uncertainty in biomass estimation.

A. *TLS for Local Nondestructive Allometry*

The findings from this study suggest that TLS is an efficient means of creating nondestructive local allometry for estimating biomass. We scanned over the span of four days, averaging three 1/10th ha plots per day. The relatively short-time expenditure for field work resulted in 329 3-D tree models (only 243 were used in this study). Other work has emphasized the cost and labor saved by using TLS in place of destructive sampling, and we see similar benefits in this approach [16].

Another clear benefit from TLS was the ability to estimate the biomass of several large trees above 70 cm that would otherwise be too costly or simply unfeasible to sample. The largest trees included in the national equations were 73 cm, as opposed to 120 cm in our TLS allometry. TLS allometry estimated modeled trees greater than 70 cm to have an average of 769 kg more biomass per tree than the Jenkins *et al.* equation estimates. The larger trees included in our allometry constrain estimates of biomass, thus reducing uncertainty in the upper diameter range. Moreover, direct modeling of large trees reduced plot uncertainty substantially, as these individuals have the highest potential for error. Further reductions in error were found across every equation using height and diameter as predictors.

TLS allometry outperformed the reported error of the Jenkins *et al.* 2003 equations. Given the scale of the Jenkins allometry, we expected this finding, as these equations encompass a much broader range of growing conditions than are found at our single site. As such, one of the major benefits and likely sources of error reduction in TLS allometry was the ability to create high-sample-size equations on a small spatial scale, limiting the impact of environmental variation in the equation. We decided to group species based on a preliminary allometric analysis by creating two genus-grouped equations with species as a categorical variable. We found species within the genera of *Quercus* and *Carya* to be statistically indistinguishable in terms of β_0 and β_1. The grouping of these individuals allowed us to increase equation sample size and reduce the number of species-specific equations needed– - ultimately leading to a more reliable single equation. We included TLS model uncertainty based primarily on past validation studies of tree volume and regional destructive measurements of wood density. These two sources of error result in TLS model uncertainty of 12.4%, a comparable error to other destructive TLS validation studies [15], [18].

While TLS provided low-uncertainty allometry in this study, there are still currently major limitations to the technology that impede widespread deployment. We collected the TLS data in

This article has been accepted for inclusion in a future issue of this journal. Content is final as presented, with the exception of pagination.

low-wind leaf-off conditions in order to clearly model the woody portion of the tree stem, but this scenario can only be achieved in certain areas. Rain and wind are also detrimental to the quality of TLS data and must be avoided if reliable volume estimates are required. Deciduous forest ecosystems have the potential to benefit greatly from TLS, while dense tropical forests present significant challenges. A dense understory in any forest will substantially reduce visibility and increase occlusion. Standardized systematic sampling schemes have been suggested [33], but a thorough analysis of occlusion in the context of QSM's has yet to be completed. Instrument choice will impact scan quality and ultimately affect the quality of TLS models and biomass estimates. We used a low-cost phase-shift TLS unit known to suffer from noise, but lower noise instruments are becoming more affordable and can improve the scan quality. Finally, uncertainty in tree-level wood density presents a major challenge in high-diversity forests and must be improved before TLS is regularly deployed in these environments.

Total plot biomass was higher and uncertainty was markedly reduced at the plot level in both TLS scenarios compared to the Jenkins *et al.* equations. Given the reduction in uncertainty across allometric equations, we anticipated lower error at the plot level, but plot uncertainty only reduced by 7.1% with TLS models, 5.7% with TLS diameter–height allometry, and 4.0% with TLS diameter allometry. However, TLS model-based plot biomass was 31.4 $\mathrm{Mg{\cdot}ha^{-1}}$ higher on average than the Jenkins equations, suggesting that the improvements to biomass uncertainty may be realized at the calibration and validation stage through higher accuracy plot-level biomass values rather than increased precision. The higher estimates of biomass density using TLS suggests that: 1) this approach is sensitive to higher biomass in larger trees; and 2) national-scale allometry may be underestimating the biomass of large trees in analogous forest types. Direct 3-D modeling captures biomass density more accurately because biomass is not estimated with allometry. Since allometry estimates the mean value of biomass for a specific diameter, extreme examples of high biomass are unlikely to be estimated accurately. Allometry has been shown to systematically under- or overestimate biomass, depending on the forest type [11], highlighting the need for targeted TLS acquisitions for improved allometry or to directly estimate large tree biomass.

B. Reducing Uncertainty in SAR and LiDAR Models

Uncertainty is rarely propagated in analyses of biomass estimation with remote sensing methods [30], and no studies to our knowledge have quantified reductions to SAR or LiDAR biomass model uncertainty using TLS. Our approach uses TLS to reduce uncertainty from allometry and calibration error. The sensor calibration error is impacted primarily by the representative nature of the metric used to predict biomass (MCH or backscatter, in this study) and the accuracy of the field biomass estimates. We emphasize that nearly every remote sensing calibration and validation method for biomass estimation relies on estimates derived from empirical models rather than known values, except rarely, when destructive sampling of trees are used after data acquisition; in essence, an allometric model is used to calibrate metrics for a remote sensing model. TLS potentially provides a means to reduce the reliance on generalized allometric models for the calibration stage, thus reducing uncertainty. Since plot-level biomass can be estimated using a range of techniques, the chosen method can potentially have a dramatic impact on the final sensor calibration [14]. By quantifying improvements in empirical model calibration and propagating uncertainty, we can make more informed decisions concerning sensor calibration plot data moving forward in estimating global forest biomass.

SAR missions can be improved with TLS, even in the presence of a high-uncertainty calibration model. The backscatter provided a higher RMSE model (39.3–46.6%), but TLS still reduced uncertainty by 7.3%, a major benefit relevant for future SAR missions, especially in forests with lower biomass density. Even still, the SAR backscatter is limited by loss of sensitivity in high-biomass forests, where the residual model error is of greater relative importance compared to plot-level allometric uncertainty. For spaceborne applications, the greatest benefits will be realized with the combination of LiDAR, PolInSAR, or TomoSAR height and backscatter metrics, allowing "wall-to-wall" estimates less affected by cloud cover. In this study, fusing LiDAR height metrics to the SAR data dramatically improved the R^2 of the calibration model from 47–56% to 73–78%. Our findings suggest that a combination of TLS biomass estimates and remotely sensed height will improve future SAR sensor calibration.

Canopy height is almost certainly the most ubiquitous metric used to estimate biomass across an extensive range of forested ecosystems [2], [3], [13], [34], [35]. We used the MCH as an analogous metric to many of the upcoming satellite missions for estimating biomass. While our LiDAR calibration is directly applicable to the GEDI and Ice-SAT II missions because of the similar technology, the same findings apply to multisensor SAR configurations used to estimate forest height. The strong relationship between height and biomass found in this study confirms the findings of the overwhelming body of publications on the subject. TLS provided the most accurate and precise estimates of plot biomass and thus reduced the residual error in the LiDAR empirical model. The Jenkins *et al.* allometry systematically underestimated biomass density and was less sensitive to high-biomass plots. The strong agreement between TLS plot biomass estimates and LiDAR-derived MCH is explained by TLS plot estimates being derived from the direct sensing of forest structure rather than the indirect Jenkins *et al.* allometry. The strength of the LiDAR relationships was not anticipated given the low pulse density (approximately 1 $\mathrm{pulse{\cdot}m^{-2}}$) of the airborne LiDAR acquisition, emphasizing the explanatory power of the MCH.

Our findings suggest that traditional allometric approaches to sensor calibration may be systematically underestimating landscape-scale biomass estimates. Across every calibration model in this study, national allometry underestimated biomass compared to TLS estimates. More TLS acquisitions are needed in an array of forest ecosystems to verify the extent and magnitude of this newly discovered bias, but a shift in biomass calibration in line with this study has major implications. Our

This article has been accepted for inclusion in a future issue of this journal. Content is final as presented, with the exception of pagination.

findings of systematic negative bias agree with recent tree-level TLS work in tropical systems [36], but we show that the impacts of these biases propagate to the plot-scale and the sensor calibration stage. Less biased TLS estimates can potentially mitigate backscatter saturation in SAR systems like NISAR or BIOMASS by increasing the range of predicted biomass (13.5% in this study), while low-biomass systems benefit from higher precision estimates. LiDAR systems such as GEDI or ICE-Sat II will be capable of estimating biomass in dense forests, but TLS may provide additional sensitivity and reduced bias in some of the highest density forests. TLS can also potentially provide less biased low-uncertainty calibration for airborne LiDAR acquisitions intended to inform spaceborne sensors.

V. Conclusion

TLS is an effective and efficient means of reducing uncertainty in calibration of remote sensing missions estimating biomass. We emphasize that the framework described is broadly applicable beyond the specific TLS system and remote sensing products used in this study. More advanced TLS systems using multiple returns and lower noise technology (e.g., time of flight) will further reduce uncertainty in biomass assessment, providing high-sample-size allometry primarily representing regional population-level variation in the tree structure. As TLS becomes more accessible, this framework can standardize biomass uncertainty assessment with a range of TLS instruments and remote sensing products in forests globally. We determined that TLS can reduce uncertainty in the future by:

1) providing a direct estimate of standing biomass by sensing woody volume, thus reducing the reliance on unrepresentative allometry;
2) allowing the development of more representative nondestructive local allometric equations for application to available plot data;
3) reducing residual variability in the SAR and LiDAR sensor calibration model stage.

TLS is unlikely to replace manual forest inventory completely, but adaptive methods may significantly improve plot-level biomass estimates for calibration and validation. Certain ecosystems such as dense tropical forests present challenges for automated TLS inventory because occlusion reduces confidence in relatively simple measurements, but high-quality single-tree biomass estimation in these systems can supplement limited allometry. Ultimately, the greatest future improvements to biomass mapping will be found with targeted TLS acquisitions in areas with nonexistent local allometric equations and high-biomass density. Finally, due to the direct dependence of sensor calibration on plot-level estimates, low-bias and uncertainty assessment with TLS has the potential to impact national and global estimates of aboveground biomass and carbon storage made with future spaceborne missions including GEDI, ICE-Sat II, NISAR, and BIOMASS.

Acknowledgment

The authors would like to thank the Smithsonian Conservation Biology Institute, especially K. Teixeira, for access and support during TLS fieldwork. The collection of TLS data would not have been possible without the help of A. Stovall, A. Foster, and B. Reyes. They would also like to thank N. Bourg, W. McShea, and all others responsible for coordinating the collection of the stem map data at SCBI in the SIGEO forest. Finally, they would like to thank L. Duncanson, L. Fatoyinbo, X. Yang, T. Vorster, and three anonymous reviewers for helpful comments and suggestions for this manuscript.

References

[1] R. A. Houghton, F. Hall, and S. J. Goetz, "Importance of biomass in the global carbon cycle," *J. Geophys. Res., Biogeosci.*, vol. 114, Sep. 2009, Art. no. G00E03.
[2] S. Saatchi *et al.*, "Benchmark map of forest carbon stocks in tropical regions across three continents," *Proc. Nat. Acad. Sci. United States Amer.*, vol. 108, no. 24, pp. 9899–9904, Jun. 2011.
[3] A. Baccini *et al.*, "Estimated carbon dioxide emissions from tropical deforestation improved by carbon-density maps," *Nature Climate Change*, vol. 2, no. 3, pp. 182–185, 2012.
[4] E. T. A. Mitchard *et al.*, "Markedly divergent estimates of Amazon forest carbon density from ground plots and satellites," *Global Ecol. Biogeography*, vol. 23, no. 8, pp. 935–946, Aug. 2014.
[5] N. Picard, L. Saint-Andre, and M. Henry, *Manual for Building Tree Volume and Biomass Allometric Equations: From Field Measurement to Prediction*. Rome, Italy: Food Agricultural Org. United Nations/Centre Coopération Int. Recherche Agronomique pour le Dévelop., Aug. 2012.
[6] J. Chave, R. Condit, S. Aguilar, A. Hernandez, S. Lao, and R. Perez, "Error propagation and scaling for tropical forest biomass estimates," *Philosoph. Trans. Roy. Soc. B, Biol. Sci.*, vol. 359, no. 1443, pp. 409–420, 2004.
[7] F. G. Hall *et al.*, "Characterizing 3D vegetation structure from space: Mission requirements," *Remote Sens. Environ.*, vol. 115, no. 11, pp. 2753–2775, 2011.
[8] D. Wickland *et al.*, "CEOS strategy for carbon observations from space," in *Proc. 40th COSPAR Sci. Assem.*, vol. 40, ch 2, 2014, pp. 34–36.
[9] S. Goetz and R. Dubayah, "Advances in remote sensing technology and implications for measuring and monitoring forest carbon stocks and change," *Carbon Manage.*, vol. 2, no. 3, pp. 231–244, 2011.
[10] L. I. Duncanson, R. O. Dubayah, and B. J. Enquist, "Assessing the general patterns of forest structure: Quantifying tree and forest allometric scaling relationships in the United States: Forest allometric variability in the United States," *Global Ecol. Biogeography*, vol. 24, no. 12, pp. 1465–1475, Dec. 2015.
[11] L. Duncanson, O. Rourke, and R. Dubayah, "Small sample sizes yield biased allometric equations in temperate forests," *Sci. Rep.*, vol. 5, Nov. 2015, Art. no. 17153.
[12] J. Chave *et al.*, "Improved allometric models to estimate the aboveground biomass of tropical trees," *Global Change Biol.*, vol. 20, no. 10, pp. 3177–3190, 2014.
[13] R. E. McRoberts, Q. Chen, G. M. Domke, G. Sthl, S. Saarela, and J. A. Westfall, "Hybrid estimators for mean aboveground carbon per unit area," *Forest Ecol. Manage.*, vol. 378, pp. 44–56, Oct. 2016.
[14] F. Zhao, Q. Guo, and M. Kelly, "Allometric equation choice impacts lidar-based forest biomass estimates: A case study from the Sierra National Forest, CA," *Agricultural Forest Meteorol.*, vol. 165, pp. 64–72, Nov. 2012.
[15] K. Calders *et al.*, "Nondestructive estimates of above-ground biomass using terrestrial laser scanning," *Methods Ecol. Evol.*, vol. 6, no. 2, pp. 198–208, Feb. 2015.
[16] A. E. Stovall, A. G. Vorster, R. S. Anderson, P. H. Evangelista, and H. H. Shugart, "Non-destructive aboveground biomass estimation of coniferous trees using terrestrial LiDAR," *Remote Sens. Environ.*, vol. 200, pp. 31–42, Oct. 2017.
[17] P. Raumonen *et al.*, "Fast automatic precision tree models from terrestrial laser scanner data," *Remote Sens.*, vol. 5, no. 2, pp. 491–520, Jan. 2013.
[18] J. Hackenberg, M. Wassenberg, H. Spiecker, and D. Sun, "Non destructive method for biomass prediction combining TLS derived tree volume and wood density," *Forests*, vol. 6, no. 4, pp. 1274–1300, 2015.
[19] J. C. Jenkins, D. C. Chojnacky, L. S. Heath, and R. A. Birdsey, "National-scale biomass estimators for United States tree species," *Forest Sci.*, vol. 49, no. 1, pp. 12–35, 2003.

This article has been accepted for inclusion in a future issue of this journal. Content is final as presented, with the exception of pagination.

[20] N. A. Bourg, W. J. McShea, J. R. Thompson, J. C. McGarvey, and X. Shen, "Initial census, woody seedling, seed rain, and stand structure data for the SCBI SIGEO large forest dynamics plot: Ecological archives E094-195," *Ecology*, vol. 94, no. 9, pp. 2111–2112, 2013.
[21] D. C. Chojnacky, L. S. Heath, and J. C. Jenkins, "Updated generalized biomass equations for North American tree species," *Forestry*, vol. 87, no. 1, pp. 129–151, Jan. 2014.
[22] *SCENE (version 5.4.4.41689)*. FARO Technol. Inc., Lake Mary, FL, USA, 2015.
[23] M. Hauglin, V. Lien, E. Nsset, and T. Gobakken, "Geo-referencing forest field plots by co-registration of terrestrial and airborne laser scanning data," *Int. J. Remote Sens.*, vol. 35, no. 9, pp. 3135–3149, May 2014.
[24] A. Othmani, A. Piboule, M. Krebs, C. Stolz, and L. L. Y. Voon, "Towards automated and operational forest inventories with T-Lidar," in *Proc. 11th Int. . LiDAR Appl. Assessing Forest Ecosyst.*, 2011, pp. 1–9.
[25] G. B. West, J. H. Brown, and B. J. Enquist, "A general model for the structure and allometry of plant vascular systems," *Nature*, vol. 400, no. 6745, pp. 664–667, Aug. 1999.
[26] P. Radtke, D. Walker, A. Weiskittel, J. Frank, J. Coulston, and J. Westfall, "Legacy tree data: A national database of detailed tree measurements for volume, weight, and physical properties," USDA Forest Service, Portland, OR, USA, Gen. Tech. Rep. PNW-GTR-931, 2015.
[27] A. Clark, D. R. Phillips, and D. J. Frederick, "Weight, volume, and physical properties of major hardwood species in the gulf and Atlantic coastal plains," USDA Forest Service, Portland, OR, USA, Tech. Rep. Res. Paper SE-250, 1985.
[28] A. Clark, D. R. Phillips, and D. J. Frederick, "Weight, volume, and physical properties of major hardwood species in the Upland-South," USDA Forest Service, Tech. Rep. Res. Paper SE-257, 1986.
[29] A. Clark, D. R. Phillips, and D. J. Frederick, "Weight, volume, and physical properties of major hardwood species in the Piedmont," USDA Forest Service, Tech. Rep. Res. Paper SE-255, 1986.
[30] Q. Chen, G. Vaglio Laurin, and R. Valentini, "Uncertainty of remotely sensed aboveground biomass over an African tropical forest: Propagating errors from trees to plots to pixels," *Remote Sens. Environ.*, vol. 160, pp. 134–143, Apr. 2015.
[31] E. T. A. Mitchard *et al.*, "Using satellite radar backscatter to predict above-ground woody biomass: A consistent relationship across four different African landscapes," *Geophys. Res. Lett.*, vol. 36, Dec. 2009, Art. no. L23401.
[32] ASF DAAC 2011, *ALOS PALSAR_Radiometric_Terrain_Corrected_high_res*. Includes Material JAXA/METI 2007, Dec. 27, 2017.
[33] P. Wilkes *et al.*, "Data acquisition considerations for terrestrial laser scanning of forest plots," *Remote Sens. Environ.*, vol. 196, pp. 140–153, Jul. 2017.
[34] G. P. Asner, "Tropical forest carbon assessment: Integrating satellite and airborne mapping approaches," *Environ. Res. Lett.*, vol. 4, no. 3, Sep. 2009, Art. no. 034009.
[35] T. E. Fatoyinbo and M. Simard, "Height and biomass of mangroves in Africa from ICESat/GLAS and SRTM," *Int. J. Remote Sens.*, vol. 34, no. 2, pp. 668–681, Jan. 2013.
[36] J. Gonzalez de Tanago *et al.*, "Estimation of above-ground biomass of large tropical trees with terrestrial LiDAR," *Methods Ecol. Evol.*, vol. 9, no. 2, pp. 223–234, Nov. 2017.

Atticus E. L. Stovall received the Ph.D. degree in environmental sciences from the University of Virginia, Charlottesville, VA, USA, in 2017, where he developed methods of improving biomass mapping through direct 3-D modeling of trees with terrestrial LiDAR.

He is a Forest Ecologist with an emphasis on LiDAR remote sensing for precision measurements of forest biomass and carbon. He quantified the uncertainty from commonly used allometric equations and how they can potentially impact airborne and spaceborne LiDAR-based biomass mapping. He also led and collaborated on projects investigating mangrove allometry in Gabon, the influence of microtopography on forest productivity in bog-lands, the relationship between fine-scale 3-D forest complexity and ecosystem productivity, and landscape scale drought mortality mapping of individual trees with airborne LiDAR.

Herman H. Shugart received the Ph.D. degree in zoology from the University of Georgia, Athens, GA, USA, in 1971.

He worked for the next 13 years in Tennessee eventually as a Senior Research Scientist at the Oak Ridge National Laboratory and as a Professor in Botany and the Graduate Program in Ecology with the University of Tennessee. In 1984, he joined the University of Virginia, Charlottesville, VA, USA, where he is currently the W.W. Corcoran Professor of environmental sciences. He has also served as a Visiting Fellow with the Australian National University (1978–1979 and 1993–1994), in Australia's Commonwealth Industrial and Scientific Research Organization, Division of Land Use Research (1982) and Division of Wildlife and Ecology (1993–1994), in the International Meteorological Institute, University of Stockholm, Sweden (1984), and in the International Institute of Applied Systems Analysis, Laxenburg, Austria (1987 and 1989). He has served as the major advisor to 24 completed master's students, 54 completed Ph.D. students, and 21 postdoctoral associates.